The Bipolar Kinesin, KLP61F, Cross-links Microtubules within Interpolar Microtubule Bundles of *Drosophila* Embryonic Mitotic Spindles

David J. Sharp,* Kent L. McDonald,‡ Heather M. Brown,* Heinrich J. Matthies,* Claire Walczak,§ Ron D. Vale,‖ Timothy J. Mitchison,¶ and Jonathan M. Scholey*

*Section of Molecular and Cellular Biology, University of California Davis, Davis, California 95616; ‡Electron Microscope Lab, University of California, Berkeley, California 94720-3330; §Medical Sciences Program, Indiana University, Bloomington, Indiana 47405; ‖Howard Hughes Medical Institute, University of California, San Francisco, California 94143; and ¶Department of Cell Biology, Harvard Medical School, Boston, Massachusetts 02115

Abstract. Previous genetic and biochemical studies have led to the hypothesis that the essential mitotic bipolar kinesin, KLP61F, cross-links and slides microtubules (MTs) during spindle assembly and function. Here, we have tested this hypothesis by immunofluorescence and immunoelectron microscopy (immunoEM). We show that *Drosophila* embryonic spindles at metaphase and anaphase contain abundant bundles of MTs running between the spindle poles. These interpolar MT bundles are parallel near the poles and antiparallel in the midzone. We have observed that KLP61F motors, phosphorylated at a cdk1/cyclin B consensus domain within the BimC box (BCB), localize along the length of these interpolar MT bundles, being concentrated in the midzone region. Nonphosphorylated KLP61F motors, in contrast, are excluded from the spindle and display a cytoplasmic localization. Immunoelectron microscopy further suggested that phospho-KLP61F motors form cross-links between MTs within interpolar MT bundles. These bipolar KLP61F MT-MT cross-links should be capable of organizing parallel MTs into bundles within half spindles and sliding antiparallel MTs apart in the spindle midzone. Thus we propose that bipolar kinesin motors and MTs interact by a "sliding filament mechanism" during the formation and function of the mitotic spindle.

Key words: mitosis • bipolar kinesin • Bim C • microtubule • *Drosophila*

SUCCESSFUL mitosis requires that genetic material is equally segregated into two daughter nuclei upon a self-organizing bipolar protein machine known as the mitotic spindle. This structure forms from two partially overlapping radial arrays of microtubules (MTs)[1] oriented with their minus-ends focused at duplicated centrosomes and their plus ends radiating outward. During early mitosis when the spindle assembles, these centrosomes and their associated asters migrate to opposite sides of the nucleus. Subsequently, the nuclear envelope breaks down, allowing MTs from each aster to interact with condensed chromosomes or with MTs of the other aster, and thus the basic lattice of the spindle forms. Chromosome segregation occurs during anaphase when spindle MTs move sister chromatids to opposite spindle poles (anaphase A) and push the spindle poles apart (anaphase B).

To explain the forces involved in spindle formation and function, McIntosh et al. (1969, 1971) proposed the sliding filament model of mitosis, in which some spindle movements were seen as analogues of the sliding of cytoskeletal elements that drive muscle contraction and flagellar beating (McDonald et al., 1977). In this model, electron-dense crossbridges observed between spindle MTs were proposed to be motor proteins capable of generating force along the surface of MTs and moving them in relation to one another. Although this sliding filament mechanism cannot account for all movements associated with spindle MTs (such as kinetochore motility), it does account nicely for the forces associated with antiparallel MTs that act on opposite spindle poles. This polar repulsive force could drive spindle pole migration during prophase, hold the poles apart during metaphase and anaphase A, and drive spindle elongation during anaphase B.

Address correspondence to Dr. Jonathan M. Scholey, Section of Molecular and Cellular Biology, 1 Shields Ave., The University of California, Davis, CA 95616. Tel.: (530) 752-2271. Fax: (530) 752-7522. E-mail: jmscholey@ucdavis.edu

1. *Abbreviations used in this paper:* BCB, unphosphorylated BimC box; cdk1, cyclin-dependent kinase 1; CSF, cytostatic factor; HPF/FS, high-pressure freezing/freeze substitution; HSS, high speed supernatant; immunoEM, immunoelectron microscopy; LB, Luria broth; MAP, microtubule-associated protein; MT, microtubule; p-BCB, phosphorylated BCB; PI, protease inhibitor; Rs, Stokes radius; TEM, transmission EM.

While their specific modes of action have not been determined, MT-based motor proteins are now known to play important roles in mitosis (Gelfand and Scholey, 1992; Barton and Goldstein, 1996; Hoyt 1994; Walczak and Mitchison, 1996). Genetic analyses, antibody microinjections, and immunodepletions from extracts have shown clearly that MT-associated motor proteins are essential for the proper formation of the mitotic spindle in a variety of organisms (see Heck et al., 1993; Wright et al., 1993; Sawin et al., 1992). Furthermore, one prominent group or subfamily of mitotic motors, the bipolar kinesins (or BimC family of kinesins), have been proposed to organize spindle poles, to contribute to pole-pole separation, and to drive spindle elongation (Enos and Morris, 1990; Hagan and Yanagida, 1990, 1992; Hoyt et al., 1992; Roof et al., 1992; Saunders and Hoyt, 1992; Heck et al., 1993; O'Connell et al., 1993; Saunders et al., 1995; Blangy et al., 1995, 1997; Straight and Murray, 1998), all of which may potentially use a sliding filament mechanism.

Although it is unclear how bipolar kinesins exert their effects in the spindle, recent work suggests that at least one member of this family could affect spindle bipolarity by cross-linking and sliding MTs by a sliding filament mechanism. Probes of *Drosophila* embryonic cytosol with pan-kinesin antibodies led to the purification of a slow, plus-end-directed, homotetrameric kinesin (Cole et al., 1994) that is structurally bipolar having two motor domains at both ends of a ~60-nm-long rod (Kashina et al., 1996a). Microsequencing and MALDI mass spectroscopy of tryptic digests revealed that this bipolar motor was, in fact, the product of the gene encoding the bipolar kinesin, KLP61F (Kashina et al., 1996b). KLP61F was discovered as a late larval lethal mutant encoding a kinesin-like protein. Interestingly, severe loss of function mutations of this bipolar kinesin are hallmarked by monoastral spindles apparently resulting from unseparated or collapsed spindle poles within proliferative tissues (Heck et al., 1993).

Based on these biochemical and genetic data, we have proposed that KLP61F and its homologues function as spindle MT cross-linkers, acting on antiparallel MTs to separate and hold apart spindle poles or on parallel MTs to drive subunit flux in kinetochore MTs (Kashina et al., 1996a). Our aim here is to test this hypothesis by immunolocalizing KLP61F within the spindles of early *Drosophila* embryos using peptide antibodies monospecific for a phospho-epitope in the tail of the motor. Given the known transport properties of the motor and the terminal phenotype of the KLP61F mutant, the determination of how the motor holoenzyme associates with MTs and the polarity of the MTs with which it interacts will provide a crucial functional link between the in vitro transport properties of the motor (Cole et al., 1994; Barton et al., 1995) and the monoastral spindles that characterize severe loss of function mutants (Heck et al., 1993).

Materials and Methods

Preparations and Care of Fly Stocks

Oregon red strains of *Drosophila melanogaster* were maintained in large farms as previously described (Ashburner, 1989; Meyer et al., 1998). In some of the immunofluorescence and electron microscopic analyses described below, flies were collected from the University of California San Francisco fly facility.

Drosophila Embryonic Tubulin Preparation

High speed supernatant (HSS) from extracts of 0–2 h *Drosophila* embryos was generated as previously described (Meyer et al., 1998). Actin and myosin were depleted from HSS by incubation with hexokinase (10 U/ml) and 0.9% glucose for 30 min at room temperature and spinning at 35,000 *g* for 30 min. The supernatant was then collected and incubated with 1 mM GTP and 20 μM taxol for 45 min, then spun through a 15% sucrose cushion (containing 100 μM GTP, 100 μM ATP, and 5 μM taxol) and spun again at 20,000 *g* for 60 min at 10°C. The pellet was resuspended in PMEG, and immediately spun again for 20 min at 60,000 *g* at 10 C. The pellets were then resuspended in PMEG containing 10 μM ATP, 10 μM $MgSO_4$, 10 μM taxol, 100 μM GTP, and 0.5 M KCl for 4 h at 4°C and spun at 130,000 *g* for 45 min at 4°C. The pellets were resuspended in PMEG containing 100 μM GTP and 10 μM taxol aliquoted and stored at −80°C. Tubulin prepared in this manner was used for antibody generation and affinity purification, described below.

Preparation of Drosophila Embryonic Tubulin Antibodies

The taxol stabilized MTs were injected into three rabbits along with Freund's complete adjuvant and a week later 10 ml of blood was taken. This occurred once a month for 5 mo. Samples from each bleed were taken and tested for reactivity with tubulin by Western blotting *Drosophila* HSS and preparations of MTs and microtubule-associated proteins (MAPs). One of the three rabbits showed a strong response to the tubulin injections.

Anti-tubulin antibodies were affinity purified on columns of affigel 15 (Biogel) coupled to *Drosophila* embryonic tubulin. After binding of the tubulin to the columns, the columns were washed 10 vol of PBS-0.5% Tween-20 (PBS-Tween) and then blocked in PBS-Tween containing 5% BSA (Sigma) for 1 h at room temperature. Next, the columns were washed with 10 vol of PBS-Tween and incubated with the antiserum diluted 1:5 in blocking solution overnight at 4°C. The columns were then washed in 20 vol of PBS-Tween. Antibody was eluted from the column with 0.1 M glycine, pH 2.7, and collected in 0.8-ml fractions into clean tubes containing 0.2 ml of 1 M Tris, pH 8.0. The OD 280 of all elution fractions was determined against a standard of the tris/glycine mixture. All fractions with an OD 280 of >0.05 were kept and dialyzed into PBS overnight at 4°C.

Design and Preparation of BCB Antibodies

Polyclonal anti-BCB peptide antibodies were raised using synthetic peptides of sequence CPTGTTPQRRDYA, corresponding to the highly conserved BCB of frog Eg5. The peptide was synthesized with and without a phospho-threonine residue at residue position 6 corresponding to the consensus cdk1 phosphorylation site (Heck et al., 1993; Sawin and Mitchison, 1995), and NH_2-terminal acetyl and COOH-terminal amide groups were included. Approximately 40 mg both peptides at >92% purity were obtained by HPLC at the UCSF biomolecular resource center where the masses of the p-BCB and BCB peptides were confirmed by mass spectroscopy. Both peptides were found to be highly water-soluble and were conjugated to KLH carrier protein (5 mg peptide/50 mg KLH). The anti-p-BCB and anti-BCB antibodies were produced by BabCo (Richmond) and specific antibodies were purified from immune sera on columns of BCB or p-BCB peptides coupled to affigel 10. Bound antibodies were eluted using 0.1 M glycine, pH 2.5, and rapidly neutralized using 1 M Tris buffer, pH 10. Antibodies were then incubated with a 100-fold excess of blocking peptide (p-BCB peptide in the case of the anti-BCB antibody and BCB peptide in the case of the anti-p-BCB antibody).

To test the reactivity of these antibodies against phospho- and unphospho-KLP61F, recombinant KLP61F (or its stalk-tail fragment) prepared as described by Barton et al. (1995) was bound batchwise to glutathione-agarose beads, the beads were washed in CSF extract buffer then incubated with M-phase or I-phase *Xenopus* egg extracts or corresponding buffer plus [^{32}P]ATP for 10 min (see below), then the beads were washed in cytostatic factor (CSF) extraction buffer, boiled in sample buffer, and analyzed by SDS-PAGE, immunoblotting with the BCB and p-BimC box antibodies, and autoradiography.

Hydrodynamic Analysis of Native and Recombinant KLP61F and Phospho-KLP61F

To analyze the hydrodynamic properties of phosphorylated and unphosphorylated native KLP61f from fly embryos, fractions prepared as described previously (Cole et al., 1994) were analyzed by immunoblotting with the anti-BCB and anti-p-BCB antibodies.

Isolation and Purification of Bacterially Expressed Full-Length KLP61F

Bacterial strain BL21(DE3) was transformed with the pRSET vector containing a full length KLP61F insert. To isolate KLP61F from the transformant, a colony from a freshly streaked plate was inoculated into Luria broth medium (LB) containing 200 μg/ml ampicillin and incubated overnight at 37°C. The culture was then diluted 1:100 with fresh LB+ containing 200 μg/ml ampicillin and grown at 37°C to an optical density of A600 = 0.80. The culture was then cooled to 25°C for 30 min and then induced for 4 h at 25°C with 0.2 mM IPTG. After washing, the cells were resuspended in lysis buffer (50 mM NaH_2PO_4, 300 mM NaCl, 10 mM imidazole, pH 8.0, 100 μM MgATP) and protease inhibitors (PIs; PMSF, leupeptin, pepstatin A, benzamidine) and then lysed. The lysate was spun at 39,000 *g* for 45 min at 4°C. The supernatant was loaded onto a column containing Ni NTA superflow resin (Qiagen Inc.) then washed with lysis buffer and wash buffer (50 mM NaH_2PO_4, 300 mM NaCl, 20 mM imidazole, pH 6.0, 100 μM MgATP and PIs). rKLP61F was eluted with 250 mM imidazole, 5 mM magnesium acetate, 2 mM EGTA, 15 mM potassium acetate, pH 7.25, 100 μM MgATP and PIs. rKLP61F containing fractions were pooled, filtered through a 0.2–2 μm Millex-GV syringe filter, and loaded onto a Biogel A-1.5 m column preequilibrated with IMEK (100 mM imidazole, 5 mM magnesium acetate, 2 mM EGTA, 15 mM potassium acetate, pH 7.25) + 300 mM NaCl, 100 μM MgATP and PIs. rKLP61F was then concentrated with high trap Q column (Pharmacia) and eluted using a step gradient from 0.1–1.0 M NaCl in IMEK. The peak fraction from this concentration step was then used for the hydrodynamic studies.

Phosphorylation of Bacterially Expressed KLP61F

While on the Ni-NTA column (see above), rKLP61F was washed with CSF-XB (10 mM Hepes, pH 7.7, 2 mM $MgCl_2$, 0.1 mM $CaCl_2$, 100 mM KCl, 5 mM EGTA, and 50 mM sucrose). 200 μl of *Xenopus* mitotic extract and 1.8 ml of CSF-XB + 2 mM ATP and 10 mM $MgSO_4$ were added followed by gentle rocking at room temperature for 20 min. The beads were then returned to 4°C and washed with wash buffer. The phosphorylated rKLP61F was then eluted and treated as stated above for further purification and concentration.

Stoichiometry

The Stokes radius, Rs, was determined for both phosphorylated and unphosphorylated rKLP61F by loading 500 μl of the peak high trap Q fraction onto a pharmacia superose-6 column preequilibrated with IMEK + 300 mM NaCl. Graphs of Rs vs. −0.5logKav were plotted and the Rs determined from these plots. The standard proteins and their stokes radii included cytochrome C (1.7 nm), carbonic anhydrase (2.0 nm), BSA (3.5 nm), beta amylase (5.4 nm), and thyroglobulin (8.5 nm). The sedimentation coefficient, S value, was determined for rKLP61F on 5-ml 5–20% linear sucrose gradients in IMEK + 300 mM NaCl, 100 μM ATP, and PIs. The gradients were overlaid with a solution containing the rKLP61F, 30 μg BSA (4.4 s), 30 μg aldolase (7.3 s), and 30 μg catalase (11.3 s). The gradients were centrifuged at 218,000 *g* for 12 h at 4°C. The gradients were determined to be linear by using a refractometer. A linear plot of the S value vs. the percent sucrose was used to calculate the S value for rKLP61F. The molecular mass of rKLP61F was calculated from the measured sedimentation values and Rs.

Immunofluorescence Analyses

Drosophila embryos were prepared for immunofluorescence with a modification of the protocol described by Theurkauf (1994). 0–2 h *Drosophila* embryos were collected on food trays and rinsed from the tray with Triton-NaCl and collected onto a 200-μm nylon mesh rinsed with water. The chorions were removed by immersion in 50% bleach in Triton-NaCl for 2 min. The embryos were then extensively rinsed in double distilled water and Triton-NaCl. The vitelline was removed by immersion in 100% heptane at room temperature for 2 min and fixed by the addition of an equal volume of fresh 37% formaldehyde for 5 min. The formaldehyde was then removed and replaced with 100% methanol. The heptane and most of the methanol were removed, the embryos were incubated in fresh 100% methanol for 2–3 h, and then rehydrated by washes in a graded methanol series and two washes in 100% PBS. The embryos were then washed in PBS-0.01% Triton X-100 (wash solution) and blocked for 30 min to 1 h in PBS-0.01% Triton X-100 containing 5% BSA (blocking solution). Primary antibodies, either rabbit anti–*Drosophila* tubulin, rabbit anti-p-BCB, rabbit anti-BCB, or mouse anti-β-tubulin (N357; Amersham Life Sciences), were diluted to a concentration of 1 μg/ml in blocking solution and incubated with the embryos at 4°C overnight. In double label experiments, embryos were incubated with the anti-phospho-KLP61F antibody for 4 h at room temperature, then the mouse anti-β-tubulin was added and the incubation proceeded overnight at 4°C. After incubation with primary antibodies, the embryos were washed, blocked as above, and incubated with secondary antibodies, either goat anti–mouse conjugated to lissamine rhodamine, goat anti–mouse conjugated to cy5 or goat anti–rabbit cy3 (Jackson ImmunoResearch) diluted in blocking solution (1:100 for lissamine rhodamine and cy 5 and 1:500 for cy 3) and incubated with embryos for 2–3 h at room temperature. The embryos were washed then incubated in 4′,6′-diamidino-2-phenylindole (DAPI; Sigma) diluted to 0.1 μg/ml in PBS-Triton, for 4–10 min, rinsed washed again, rinsed with 100% PBS, and mounted in *p*-phenylenediamine (Sigma) 10 mg/ml in 90% glycerol/PBS. Secondary antibody alone controls were used for all staining conditions. Embryos were visualized on a Leica TCS NT confocal microscope. Images were acquired by averaging 16–32 scans of a single optical section with the pinhole opened for optimal resolution.

Preparation for EM and ImmunoEM

Samples were prepared for EM by high pressure freezing and freeze substitution as described previously (McDonald, 1994). Fixed embryos were embedded in Eponate 12/Araldite (Ted Pella) for standard Transmission EM (TEM) or immunoEM or in LR-White (Ted Pella) for immunoEM. 35–50-nm sections were collected on an Ultracut T microtome (Leica) and picked up on copper grids coated with 0.3–0.5% formvar (Electron Microscopy Sciences) for standard TEM or on nickel grids (Ted Pella) coated with carbon and 0.5% formvar. For standard TEM, sections were post stained for 5 minutes in 2% uranyl acetate/70% methanol and 4 min in 0.5% lead citrate.

For immunoEM, sections were blocked in 5% BSA, 0.1% fish gelatin (Sigma) in PBS-0.05% Tween-20 for 30 min (blocking buffer), incubated with primary antibody (either rabbit anti-p-BCB or BCB antibodies diluted to 50 μg/ml or rabbit anti-tubulin diluted to 10 μg/ml in blocking buffer) for 1.5–2 h. Sections were rinsed in PBS-Tween then PBS and incubated in secondary antibodies (goat anti–rabbit IgG $F(ab')_2$ [H+L]) conjugated to either 5 or 10 nm gold particle; Ted Pella) diluted 1:20 in blocking buffer for 1 h. Sections were washed as before, incubated in 0.5% glutaraldehyde in PBS for 5 min then rinsed in PBS and water. Sections were post stained in 2% uranyl acetate in 70% methanol for 5 min and in lead citrate for 4 min. Samples were visualized on a Philips 410 LS transmission electron microscope. Identically treated samples were stained with secondary antibody only as controls that in all cases revealed no labeling pattern. Sections labeled with the BCB antibodies revealed only background labeling as well. Digital image enhancement of gold-labeled spindles was done with Adobe Photoshop 5.0 on scanned photographs.

MT Tracking and Reconstruction

MTs were tracked using markers and plastic overlays as described in McDonald et al. (1977).

Results

Mitosis in Early Drosophila Embryos

To understand the mechanism of action of the bipolar kinesin, KLP61F, in *Drosophila* early embryos it was important to determine the organization of the mitotic spindle components with which the motor might associate. To accomplish this, we used immunofluorescence and EM to analyze the organization of spindle MTs and the changes

in overall spindle morphology that occur throughout mitosis (Figs. 1 and 2).

Fig. 1 shows confocal immunofluorescence of embryos immunostained with a rabbit polyclonal antibody raised against embryonic *Drosophila* MTs (see Materials and Methods) and the DNA stain DAPI. These images suggest that as prophase begins, duplicated centrosomes split and migrate away from the embryo surface, traveling down opposite sides of the nucleus (Fig. 1 A). The nuclear envelope remains intact throughout prophase (Oegema et al., 1995; Fig. 1 A, inset) and very little or no tubulin staining is observed in the nuclear region. By metaphase (Fig. 1 B), the nuclear envelope has fenestrated at the poles (Stahfstrom and Staehelin, 1984), microtubules have entered the nuclear region and the chromosomes have aligned at the metaphase plate. Dense bundles of MTs are observed in the half spindles while very few astral MTs are visible. The overall morphology of the metaphase spindle is fusiform and the average spindle length is ~12 μm. Fig. 1, C and D show the tubulin staining pattern from an embryo in which anaphase A (C) has been completed in all nuclei, but only a subset have undergone anaphase B (D). In panel C, sister chromatids have moved completely to opposite poles, yet the length of the spindles, pole-pole, range from 12 to 14 μm, similar to metaphase. The spindles shown in Fig. 1 D, on the other hand, have clearly elongated, reaching lengths of ~17–18 μm. Note that the decondensation of DNA begins during anaphase B. Also note the distinct change in the morphology of the interzone (region of the spindle lying between the separated chromosomes). Before spindle elongation, the region corresponding to the interzone is fusiform as in metaphase, however, as the spindle elongates the interzone becomes straight edged. We use this change in spindle geometry to distinguish anaphase A from B in the subsequent fluorescence analyses of KLP61F localization (below). One feature of the anti-tubulin immunofluorescence shown here and in other studies is that during both metaphase and anaphase, very few MTs cross the midzone and bridge the half spindles. However, the EM analyses shown below show abundant MTs crossing the midzone suggesting that antigenic sites are masked in immunofluorescence images.

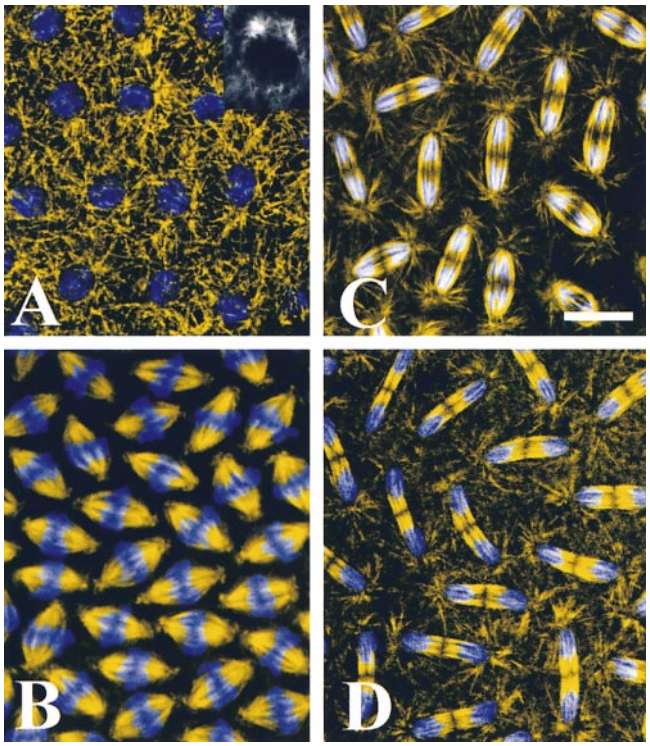

Figure 1. Mitosis in the syncytial blastoderm of early *Drosophila* embryos. Confocal immunofluorescence images of embryos immunostained with an antibody raised against *Drosophila* embryonic tubulin (yellow) overlaid with the corresponding DNA stain DAPI (blue). (A) Prophase. The chromosomes have begun to condense and centrosomes have separated significantly toward opposite sides of the nucleus. (A, inset) Cross sectional view of a prophase nucleus showing only tubulin immunofluorescence. (B) Metaphase. MTs have entered the nuclear region, and chromosomes have aligned along the metaphase plate. (C) Anaphase A. The sister chromatids have separated to opposite spindle poles but the spindles have not elongated. (D) Anaphase B. The spindles have elongated to an average length of 17.5 μm. Note that the central spindle is no longer fusiform but straight-edged. Bar, 7.6 μm.

Ultrastructural Analysis of Metaphase and Anaphase Spindles Preserved by High Pressure Freezing and Freeze/Substitution

An ultrastructural description of mitotic spindles from several stages in *Drosophila* syncytial blastoderms has been reported previously (Stahfstrom and Staehelin, 1984). However, the size of these embryos and rapid rate of mitosis during this stage of development results in a great deal of ultrastructural damage during fixation. Therefore, the use of EM to localize low abundance and easily extractable proteins requires preservation methods of a quality exceeding standard chemical fixation (McDonald, 1994). To minimize the potential extraction or mislocalization of KLP61F motors during specimen preservation, we have prepared our samples for EM by high-pressure freezing/freeze substitution (HPF/FS; for a review of this technique see Steinbrecht and Mueller, 1987; McDonald, 1994; Kiss and Staehelin, 1995). In this method, whole embryos are frozen under pressure then dehydrated and fixed simultaneously at low temperatures to preserve cellular structures rapidly and evenly with minimal extraction. (In contrast to cryofixation, in which unfixed frozen embryos are embedded or viewed on cold stage, the preparation of embryos by HPF/FS allows structures such as MTs or the nuclear envelope to be visualized easily.)

Fig. 2 is shown to illustrate, in fine detail, the organization of spindle microtubule bundles and poles after preservation by HPF/FS. Fig. 2 A shows a bundle of MTs running from the pole to the chromosome at the metaphase plate. These MTs end on an electron-dense halo, presumably the kinetochore and its corona, extending as a bolus from the chromosomes. Interestingly, no kinetochores observed were overtly trilaminar as has been reported in other systems (for review see Brinkley, 1990). Fig. 2, B and C show bundles of MTs that bridge the half spindles during metaphase and anaphase, respectively. Note that in contrast to immunofluorescence, EM clearly reveals abundant midzonal microtubules suggesting that the lack of

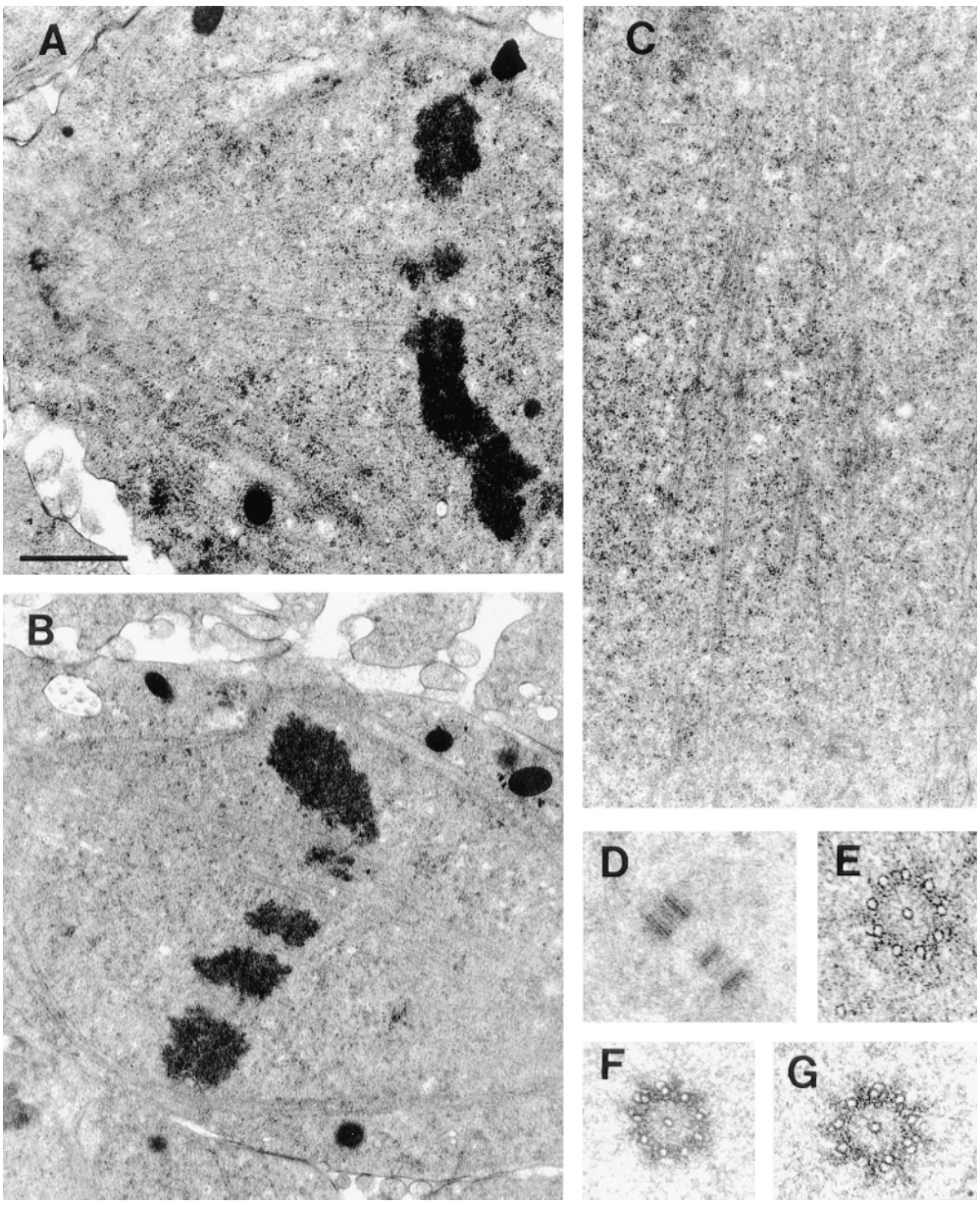

Figure 2. Detailed ultrastructure of MT bundles and spindle poles during mitosis. (A) Kinetochore MT bundles. (B) Interpolar MT bundles during metaphase. (C) Interpolar MT bundles during anaphase. D–G show the organization and structure of centrioles throughout mitosis. (D) Spindle poles contain two orthogonally positioned centrioles. The image shown is from the pole of a metaphase spindle. (E) During prophase, each centriole consists of nine singlet MTs around a central singlet MT. (F) by metaphase, the centrioles become much more electron dense and some of the outer MTs begin to form doublets. (G) In anaphase, doublets continue to form on the outer MTs. The standard organization of centrioles, nine outer triplets offset in a barrel shape, is never observed in *Drosophila* early embryos. Bar: (A) 1.3 μm; (B) 1.5 μm; (C) 1.1 μm; (D) 1.2 μm; (E–G) 0.3 μm.

anti-tubulin fluorescence in the midzone, shown in Fig. 1, results from the masking of antigenic sites. Similar bundles have been identified in vertebrate spindles and have been termed interpolar MT bundles because the entire MT bundle runs from pole to pole (although individual MTs in the bundles do not; Mastronarde et al., 1993). Here, the term interpolar MT bundles will be used to describe bundles of MTs that traverse the spindle midzone and extend into each half spindle.

Fig. 2, D–G show the organization and overall preservation of spindle poles during different stages of mitosis. Throughout the cell cycle, the most prominent structural feature of spindle poles is two orthogonally positioned centrioles (Fig. 2 D). In prophase, centrioles consist of nine outer singlet MTs plus one central singlet (Fig. 2 E). By metaphase, they become increasingly electron dense and doublets can be seen forming on some of the outer MTs. In anaphase, more doublets can be seen on the outer nine MTs and the electron density remains similar to that observed in metaphase. The organization and preservation of MT bundles and spindle poles shown in Fig. 2 is characteristic of all the samples used in this study and reinforces our confidence in the use of HPF/FS for our immunoEM analyses.

Interpolar MT Bundles Consist of Overlapping MTs Emanating from Opposite Poles

Because of their position in relation to the spindle poles, the interpolar MT bundles in *Drosophila* early embryonic spindles (described above) may be sites for MT-MT interactions that play a role in centrosome positioning. To gain a sense of the organization of the MTs and extent of half spindle overlap within these bundles, a representative in-

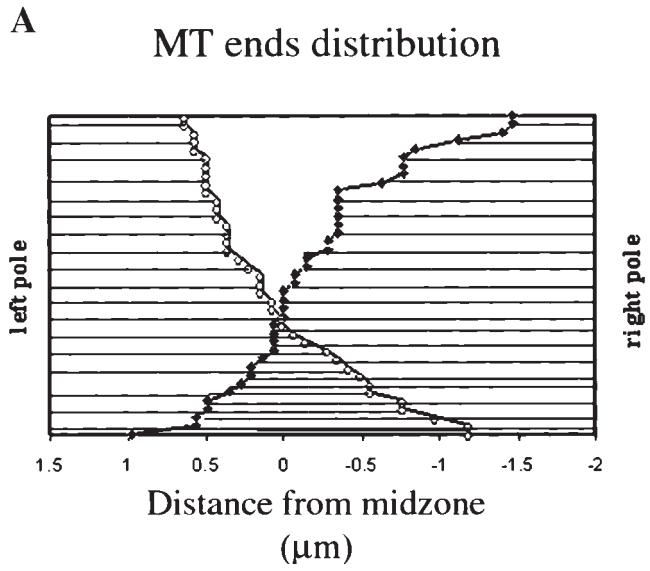

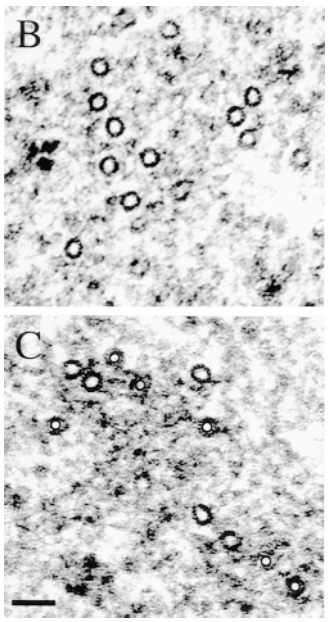

Figure 3. The MTs within interpolar MT bundles are parallel near the poles and antiparallel in the midzone. An interzonal MT bundle from a spindle beginning anaphase B was reconstructed from serial cross-sections to determine its MT polarity pattern. (A) The distribution of MT plus-ends in the reconstructed interpolar MT bundle. Individual MTs are represented by horizontal lines. The position of the plus-ends of MTs emanating from the left pole are indicated by open circles and those from the right are indicated as solid diamonds. The MTs from each half spindle are arranged top to bottom in order of increasing length in order to show the extent of possible MT overlap. (B and C) Cross-sectional profiles of the reconstructed bundle near the poles (B) and at the midzone (C). In C, MTs emanating from one pole are marked in the center with a black circle, while those from the other are not. Bar, 70 nm.

terpolar bundle was reconstructed from serial cross-sections through a mitotic spindle just beginning anaphase B, as determined by morphology and pole-pole length (Fig. 3). The results of this reconstruction are shown schematically in Fig. 3 A. Similar to other systems (McDonald et al., 1977; Euteneuer et al., 1982; Mastronarde et al., 1993; Winey et al., 1995), parallel MTs (MTs from the same pole) predominate near the poles, while antiparallel MTs are present in the midzone and extend ~1–1.5 μm into each half spindle (Fig. 3 A). Fig. 3, B and C show cross-sectional profiles of the MTs in this bundle near the poles (B) and at the midzone (C), respectively. Surprisingly, MTs are more closely associated and appear more ordered near the poles while, in the midzone, MTs are organized into numerous small sets of 2–4 MTs surrounded by an electron-dense material. Antiparallel MTs spaced 50–100 nm apart often run adjacent to one another and electron-dense crossbridges between both parallel and antiparallel MTs are often visible.

Immunodetection of Phosphorylated KLP61F

To detect KLP61F motors in the mitotic spindle, we raised anti-peptide antibodies that react with a 12-residue segment of the Bim C box located within the tail of KLP61F (Heck et al., 1993). It has been proposed that a threonine residue within the Bim C box is phosphorylated by the mitosis-promoting kinase, cdk1/cyclin B that targets bipolar kinesins to spindles (Sawin and Mitchison, 1995; Blangy et al., 1995). We prepared antibodies using both BCB and p-BCB peptides and determined that these antibodies discriminate between the phosphorylated and unphosphorylated forms of KLP61F.

Both antibodies react specifically and with high affinity with a single band in *Drosophila* syncytial blastoderm cytosol at the predicted molecular mass for KLP61F (Fig. 4 A; antibodies raised against recombinant KLP61F [Barton et al., 1995] react with the same band on immunoblots [data not shown]). However, Fig. 4 B shows that only the BCB antibody reacts with untreated bacterially expressed KLP61F (rKLP61F), while the p-BCB antibody reacts with rKLP61F only after its phosphorylation by incubation with M-phase *Xenopus* extracts (lane M) and does not react with untreated rKLP61F (lane U) or with rKLP61F

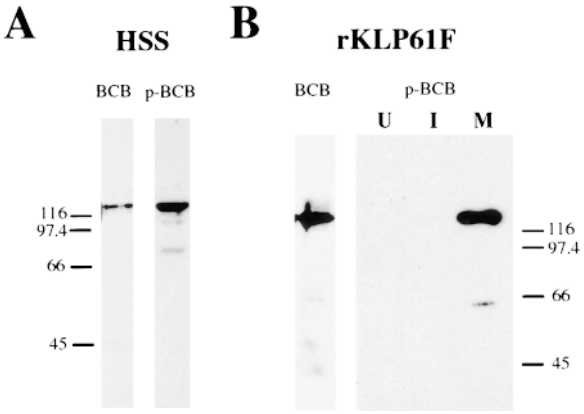

Figure 4. Characterization of the unphospho- and phospho-KLP61F antibodies. (A) Western blot of *Drosophila* 0–2-h embryonic cytosol probed with the anti-BCB and p-BCB antibodies. Both antibodies react specifically with the KLP61F polypeptide in *Drosophila* syncytial blastoderm cytosol, however, at equivalent antibody concentrations, the p-BCB antibody shows more intense staining. (B) Western blots of bacterially expressed, recombinant KLP61F before and after phosphorylation by incubation with *Xenopus* M-Phase extracts, probed with the BCB and p-BCB antibodies. While the BCB antibody reacts with untreated recombinant KLP61F (rKLP61F), the p-BCB antibody only reacts specifically with rKLP61F after it has been phosphorylated in M-phase extracts (lane M) and does not react with untreated KLP61F (lane U) or with recombinant KLP61F treated with matched interphase extracts (lane I).

Table I. Hydrodynamic Properties of KLP61F

	S value	Rs (nm)	MW	Subunits
			kD	
Native fly embryo KLP61F				
Phospho	7.8	15.6	504	4.1
Unphospho	7.8	15.6	504	4.1
Recombinant KLP61F				
Phospho	7.3	14.9	444	3.6
Unphospho	7.6	15.1	472	3.8

treated with matched interphase extracts (lane I). Parallel experiments using radiolabeled ATP revealed that the rKLP61F in lane M was phosphorylated ~4.4-fold relative to the rKLP61F in Fig. 4, lane I. Based on these results, we will subsequently refer to the BCB antibody as anti-unphospho-KLP61F and the p-BCB antibody as anti-phospho-KLP61F.

Using these antibodies to probe the phosphorylation state of native and recombinant KLP61F, we determined that the phosphorylation of KLP61F does not appear to affect the homotetrameric state of KLP61F motors in vitro, as both phospho- and unphospho-KLP61F appear to be homotetrameric based on hydrodynamic analyses (Table I). This suggests that the oligomeric state of the motor that we immunolocalized using these antibodies (below) is likely to be homotetrameric.

KLP61F Localizes to Mitotic Spindles in a Phosphorylation-dependent Manner

To determine the general localization of both phospho- and unphospho-isoforms of KLP61F within *Drosophila* syncytial blastoderms, we used the anti-KLP61F antibodies described above for immunofluorescence analyses. Fig. 5 shows confocal immunofluorescence images of embryos stained with the anti-unphospho-KLP61F overlaid with DAPI staining to indicate the relative position of DNA. Throughout mitosis, unphospho-KLP61F is diffuse and cytoplasmic, displaying no discernible association with MT arrays, nuclei, or spindles.

Embryos stained with anti-phospho-KLP61F show a markedly different staining pattern (Fig. 6). During interphase (Fig. 6 A), phospho-KLP61F staining is punctate and concentrated in the nucleus. This same pattern is observed in prophase (Fig. 6 B), after the centrosomes have separated but before nuclear envelope breakdown. However, on occasion, a very faint but noticeable dot just next to the nucleus can be seen. Double labeling with anti-tubulin antibodies indicate that these dots colocalize with the centrosome (not shown). Little or no colocalization with the microtubule bundles rimming the nuclear envelope or between the centrosomes is observed (not shown). By metaphase, after the fenestration of the nuclear envelope (Fig. 6 C), the phospho-KLP61F staining localizes to the spindle and appears filamentous. Phospho-KLP61 F is particularly concentrated on the half spindles and densely stained bridges between the half spindles in the midzone (Fig. 6 C, arrow). A slightly less concentrated staining is also visible at the poles and a grainy cytoplasmic staining is present. As the chromosomes begin to separate during anaphase A (Fig. 6 D), phospho-KLP61F staining resembles metaphase, with the most intense staining on the half spindles and filamentous bridges between the half spindles in the midzone. Interestingly, very little or no phospho-KLP61F staining can be seen on the astral MTs that begin to emanate from the poles at the onset of anaphase (see Fig. 1 C). By anaphase B (Fig. 6 E; see interzone morphology in Fig. 1 D) the staining pattern of the motor changes dramatically, as nearly all of the phospho-KLP61F is present in the spindle between the separating nuclei. Again, filaments of phospho-KLP61f staining cross the midzone while little or no staining is associated with the spindle poles and astral MTs or within the daughter nuclei. In telophase (Fig. 6 F), as the nuclear envelopes reform around daughter nuclei, phospho-KLP61F is most pro-

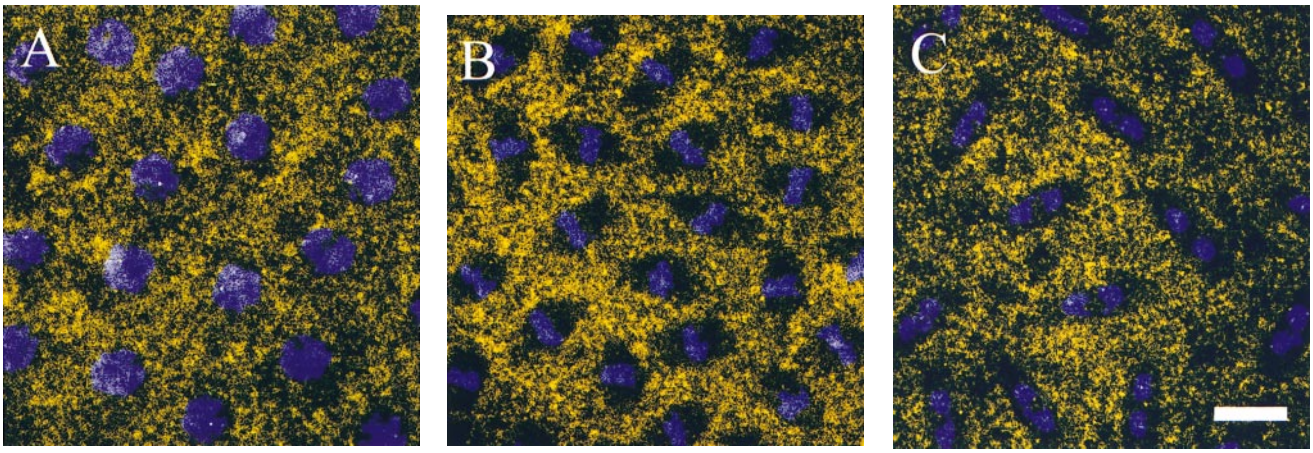

Figure 5. Unphospho-KLP61F is excluded from mitotic spindles in *Drosophila* early embryos. Confocal immunofluorescence images of *Drosophila* early embryos stained with the unphospho-KLP61F antibody (yellow) and DAPI (blue). Throughout the cell cycle, the localization of unphospho-KLP61F is cytoplasmic and does not appear associated with MTs. (A) Prophase. Before nuclear envelope breakdown, unphospho-KLP61F is specifically excluded from the nuclear region. (B) Metaphase. Once the metaphase spindle has formed, unphospho-KLP61F staining is excluded from the spindle. (C) Anaphase. The exclusion of unphospho-KLP61F from the spindle persists through anaphase. Bar, 12 μm.

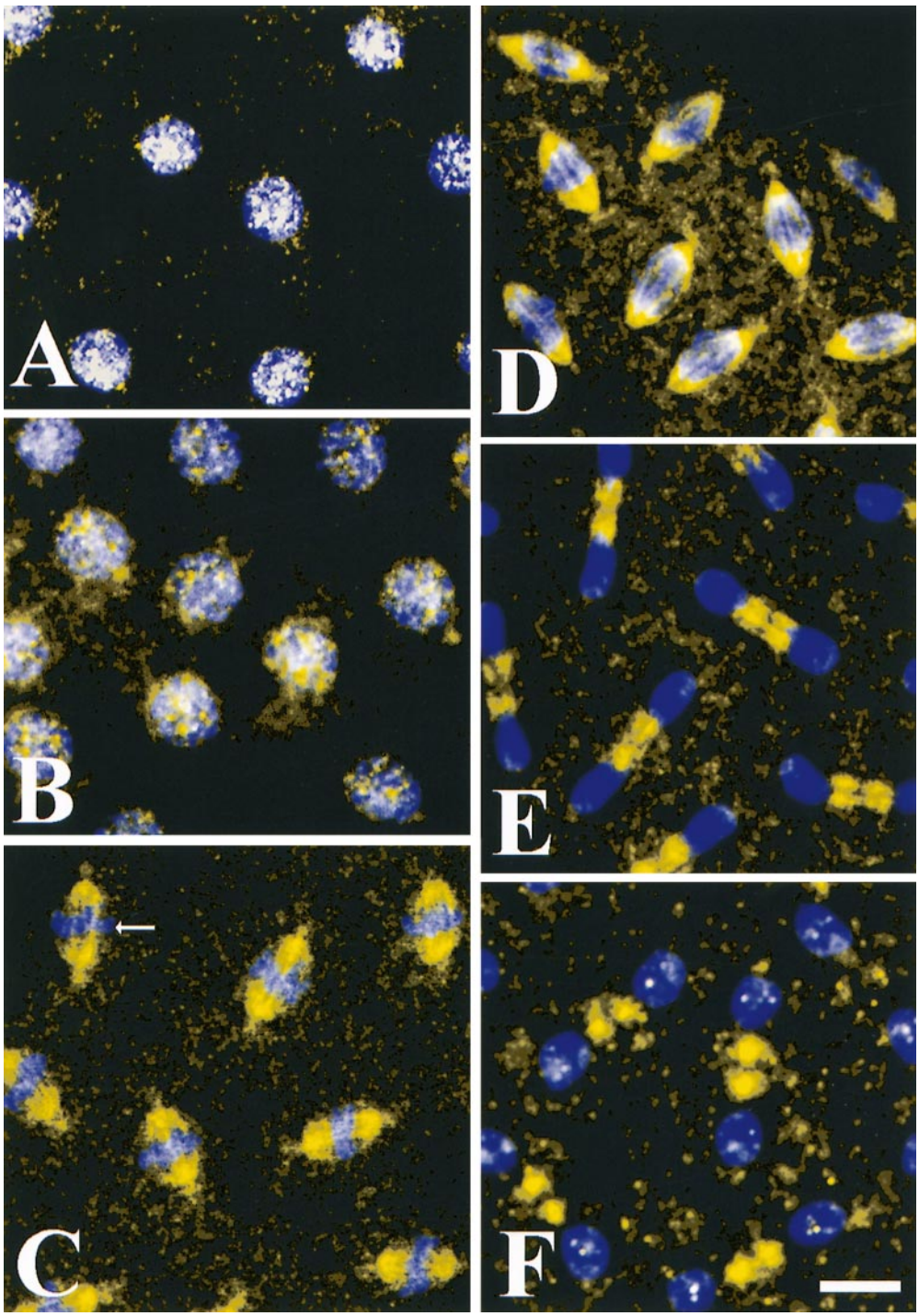

Figure 6. Phospho-KLP61F is sequestered in the nucleus during interphase and prophase and it associates with the mitotic spindle during metaphase and anaphase. Confocal immunofluorescence images of *Drosophila* early embryos stained with the anti-phospho-KLP61F antibody (yellow) and DAPI (blue). White indicates high overlap. (A) In interphase, before mitosis, phospho-KLP61F is concentrated in nuclei and overlaps significantly with DNA. (B) In prophase, before nuclear envelope breakdown, phospho-KLP61F is still concentrated in the nuclei. At this point, some staining is also detectable in the cytoplasm and perhaps on centrosomes but not on cytoplasmic microtubules. (C) In metaphase, phospho-KLP61F is now concentrated on the half spindles and on dense filaments bridging the half spindles (arrow). (D) In anaphase A, phospho-KLP61F is still concentrated on the spindles as well as on filaments bridging the half spindles. (E) In anaphase B, nearly all of the phospho-KLP61F is now concentrated in the spindle interzone, while the spindle poles and astral MTs show very low phospho-KLP61F staining. (F) In telophase, phospho-KLP61F is concentrated at two distinct punctae oriented between the daughter nuclei. Often, smaller punctae can be seen in the reforming daughter nuclei, as well. Bar, 10 μm.

nounced on two adjacent patches on the remnants of the central spindle. Close examination of the phospho-KLP61F staining pattern in the daughter nuclei also reveals that bright punctae begin to form within them. Based on these data, we conclude that, similar to its Eg5 homologues from frog and human (Sawin and Mitchison, 1996; Blangy et al., 1996), KLP61F associates with the mitotic spindle in a phosphorylation dependent fashion. Moreover, phospho-KLP61F motors associate with "filaments" crossing the spindle midzone that we believe correspond to the interpolar bundles as determined by EM (below).

Phospho-KLP61F Does Not Associate Equally with All Spindle MTs

The localization of phospho-KLP61F to distinct spindle regions may provide information about the subsets of MTs upon which the motor acts. Conversely, it may simply mirror differences in tubulin concentration within the spindle. To address this, Fig. 7 shows confocal immunofluorescence overlaying anti-phospho-KLP61F staining with anti-β-tubulin. Instead of determining the concentration of phospho-KLP61F throughout the spindle in absolute

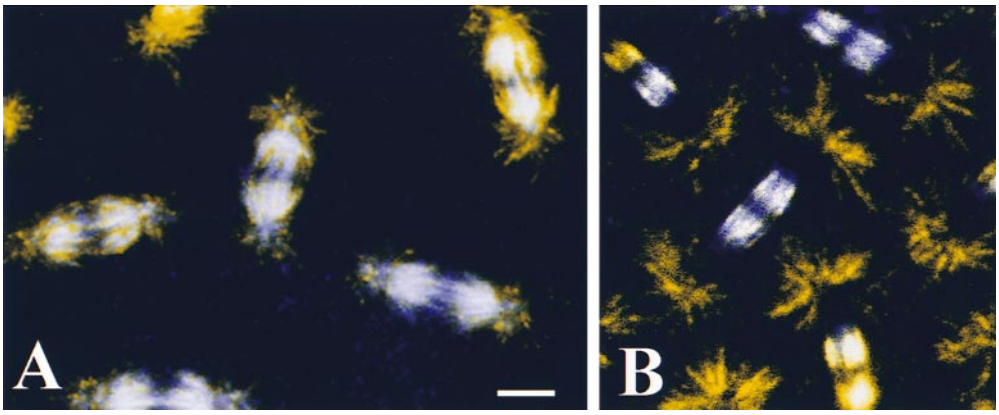

Figure 7. Relative distribution of phospho-KLP61F and tubulin in the mitotic spindle during metaphase and anaphase B. Confocal immunofluorescence images showing anti-phospho-KLP61F staining (blue) overlaid on anti β-tubulin (yellow) staining. In these images, yellow indicates the regions of the spindle in which the relative intensity of tubulin immunofluorescence is disproportionately high compared with phospho-KLP61F, white indicates the regions of relatively equal tubulin and phospho-KLP61F concentrations and blue indicates regions in which the intensity of phospho-KLP61F immunofluorescence is disproportionately high compared with tubulin. (A) In metaphase very little phospho-KLP61F colocalizes with astral MTs while the central spindle shows a high degree of overlap. The spindle midzone appears blue indicating a disproportionately high relative concentration of phospho-KLP61F to tubulin. (B) In anaphase B, nearly all of the KLP61F is concentrated in the interzone and very little is detected on chromosomes, spindle poles or astral MTs. Again, some regions of blue are apparent in the midzone indicating that phospho-KLP61F staining is disproportionately higher than tubulin staining. Bar, 5.7 μm.

terms, these images show the relative fluorescence intensity of phospho-KLP61F when compared with MTs. During metaphase (Fig. 7 A), the region of the half spindles between the poles generally shows relatively equal intensity for tubulin and phospho-KLP61F fluorescence. In contrast, the poles and astral MTs display disproportionately low phospho-KLP61F staining whereas the interpolar MT bundles crossing the midzone display disproportionately high phospho-KLP61F fluorescence. Somewhat similar results are obtained as the spindle elongates during anaphase B (Fig. 7 B), as the poles and astral MTs display disproportionately low phospho-KLP61F and bundles of MTs traversing the midzone display disproportionately high phospho-KLP61F staining. However, in metaphase some phospho-KLP61F staining is visible at the poles while, during anaphase B, polar localization of phospho-KLP61F is nearly undetectable. These data support the hypothesis that phospho-KLP61F is associated with "filaments" corresponding to interpolar MT bundles and becomes concentrated in the region of these bundles containing antiparallel MTs.

Visualization of KLP61F Associated with Interpolar Bundles of MTs by ImmunoEM

Although our immunofluorescence analyses indicate that phospho-KLP61F is present in the spindle, they cannot resolve whether the motor associates directly with individual spindle MTs. We performed immunoEM analyses using our anti-phospho-KLP61F antibody in order to examine the spatial relationship between the bipolar kinesin and MTs. Because the antibody is specific for a phospho-epitope in the tail of KLP61F these analyses allow us to examine not only whether phospho-KLP61F associates with spindle MTs but also how it is positioned relative to them by determining the position of the tail.

Fig. 8 shows the results of anti-phospho-KLP61F immunostaining performed on thin sections from embryos undergoing either metaphase (Fig. 8, A–D) or anaphase B (Fig. 8, E and F) labeled with secondary antibodies conjugated to 10- or 5-nm gold particles. The images shown in Fig. 8, A–C and E are from embryos embedded in the standard immunoEM resin, LR-White. At low magnification (Fig. 8, A and E), the staining patterns observed are consistent with the immunofluorescence shown above. Dense staining of the metaphase half spindles (Fig. 8 A), the anaphase interzone (E), and filaments bridging the midzone in both spindles (A and E) is observed. Gold labeling is also present on the poles but does not appear as concentrated as in the half spindles. The gold particle density in the spindle region is extremely high in relation to the cytoplasm (~253 vs. 7.3 particles/μm^2 during metaphase and ~237 vs. 54 particles/μm^2 during anaphase B in spindles vs. cytoplasm, respectively). Higher magnification reveals that gold labeling is clearly concentrated on or near interpolar MTs in the metaphase midzone (Fig. 8, B–D) and anaphase interzone (F). Note that immunolabeling only occurs at the surface of the section (Stierhof et al., 1991) and this accounts for the patchy labeling of MTs. The close juxtapositioning of gold particles to MTs was best seen in sections from embryos embedded in Eponate 12/Araldite resin to optimize spatial resolution (Fig. 8, D and F). Fig. 8 D shows the staining pattern along a metaphase interpolar MT bundle and Fig. 8 F shows the labeling of a bundle from an anaphase spindle. In both images it is apparent that the gold labeling is located extremely close to the surface of MTs. Measurements of the distance between gold particles and MTs indicates that, on average, gold particles lie ~9 and 7 nm from the surface of MTs during metaphase and anaphase, respectively (see Table II).

Anti-phospho-KLP61F Antibodies Associate with Crossbridges between MTs

Our structural model posits that KLP61F motors cross-

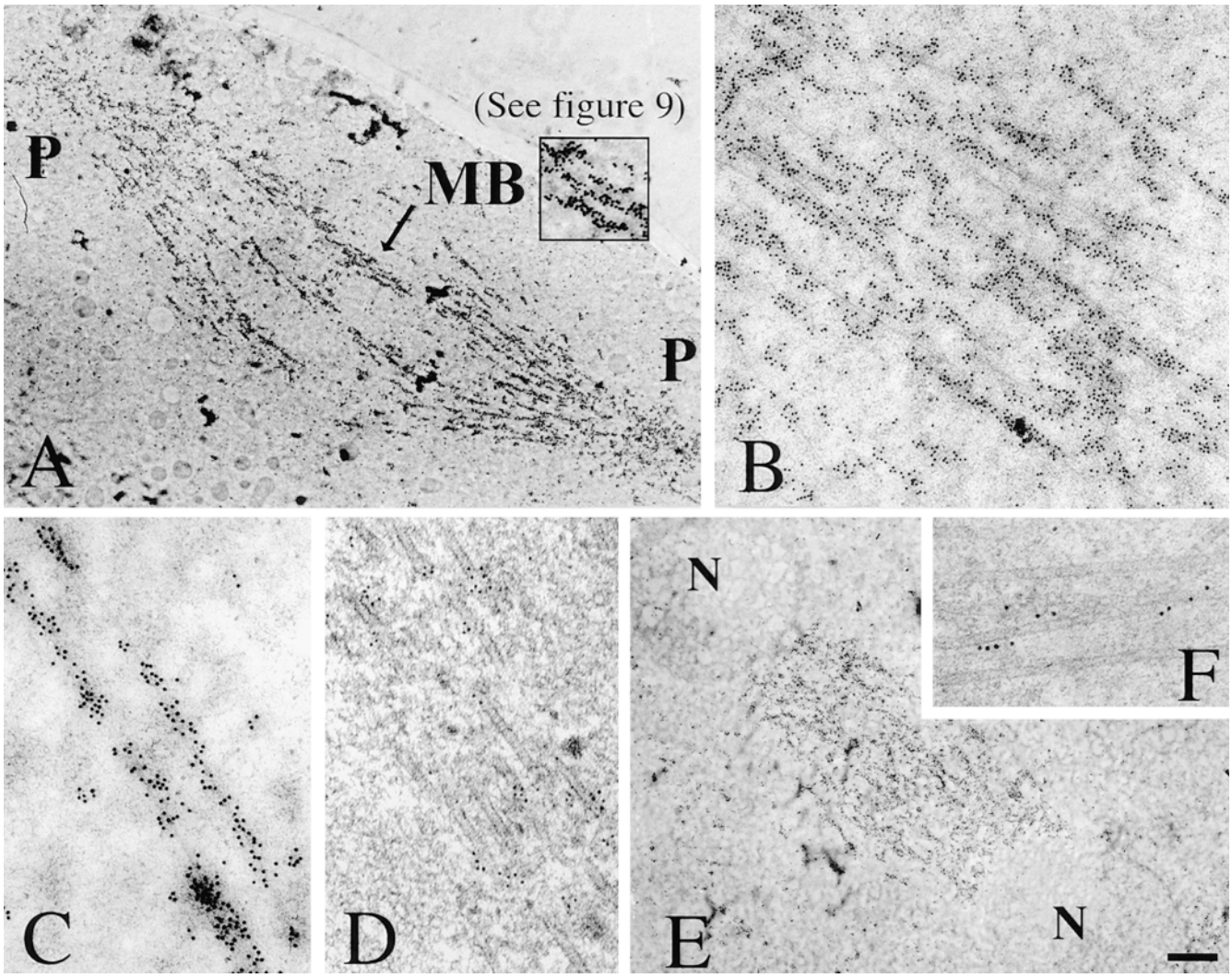

Figure 8. Visualization of phospho-KLP61F associated with interpolar MT bundles in metaphase and anaphase spindles. EMs of thin sections of *Drosophila* syncytial blastoderms preserved by HPF/FS and immunostained with the anti p-BCB antibody and gold conjugated secondary antibodies. (A and E) Phospho-KLP61F staining pattern on whole metaphase and anaphase spindles, respectively, from embryos embedded in LR-White and labeled with secondary antibodies conjugated to 10 nm gold (P, spindle poles; MB, interpolar MT bundle; N, separating daughter nuclei). (A inset) Higher magnification of the interpolar bundle (MB) indicated by the arrow and shown in digitally enhanced contrast in Fig. 9. When this region is enhanced for contrast, the gold can be seen to associate with electron-dense crossbridges between microtubules (Fig. 9). (B and C) Higher magnification of the immunostaining pattern in metaphase spindle midzones. (D and F) Phospho-KLP61F immunostaining pattern on interpolar MT bundles during metaphase and anaphase B, respectively, from embryos embedded in Eponate 12/Araldite and stained with secondary antibodies conjugated to 5 nm gold to increase the precision with which the proximity of the gold to the MT can be determined. Gold particles are closely associated with the surface of MTs within these bundles. Bar: (A and E) 1.3 μm; (B) 320 nm; (C) 160 nm; (D and F) 100 nm.

link interpolar MTs as bipolar homotetramers. A prediction of this model is that our anti-phospho-KLP61F antibody should lie at spacings ~60 nm apart at opposite ends of MT crossbridges (Fig. 9 A). In support of this hypothesis, we observed gold-labeled MT cross-links when the images shown in Fig. 8 were digitally enhanced to increase contrast. Fig. 9 B (top panel) shows a region of the anti-phospho-KLP61F-labeled interpolar MT bundle indicated by the inset in Fig. 8 A. In this image, a portion of the gold particles can be seen clearly associated with electron-dense filaments running between adjacent MTs (red arrows point down the long the axis of these filaments). In many cases, such as the one shown, these filaments are extremely numerous, producing a formation similar to rungs on a latter. Similar crossbridges were observed in different regions of multiple spindles and all showed nearly identical morphologies (Fig. 9 B, bottom panels). We identified

*Table II. Average Distance of Gold Particles from the Nearest MT**

Mitotic stage	Average distance between gold and MT
Metaphase	9.4 ± 6.2 nm
Anaphase	7.6 ± 4.5 nm

*For each stage these numbers were derived by averaging the distances between 500 gold particles from the nearest microtubule. Five different spindles were examined (100 gold particles/spindle).

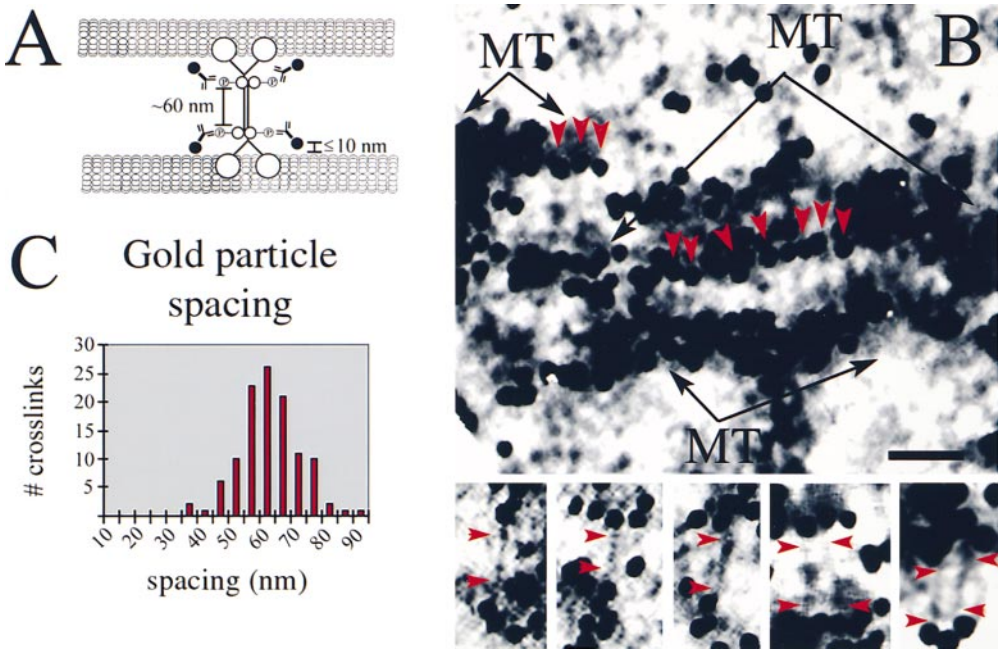

Figure 9. Antiphospho-KLP61F antibodies associate with electron-dense crossbridges between spindle microtubules. (A) Schematic illustration showing the predicted immunogold labeling pattern in spindles stained with the anti-phospho-KLP61F antibody. Based on the predicted position of the Bim C boxes on a bipolar KLP61F holoenzyme, gold particles should be spaced ~60 nm apart on electron-dense MT crossbridges. Note that although the antigenic sites are spaced ~60 nm apart, the crossbridges themselves are longer. Furthermore, the gold should be closely juxtaposed with microtubules, lying, on average, within 10 nm from the microtubule surface, just as we observe, (see Table II). (B) Observed gold labeling pattern in the spindle midzone. (Top) The image shown is the inset from Fig. 8 A with digitally enhanced contrast. (MT, microtubules, red arrowheads point down the long axis gold particle associated crossbridges.) (Bottom) Gallery of gold-labeled crossbridges. Red arrowheads indicate the two ends of the crossbridge adjacent to the associated gold particles. (C) Histogram of cross-link lengths. 115 MT crossbridges with gold particles associated at both ends were identified from two spindles and the length between the center of each gold particle was measured. The spacing ranged between 35 and 95 nm with a mean ~60-65 nm. Bar: (B, top) 60 nm; (B, bottom) 45 nm.

115 of these filaments that were decorated with gold particles on both ends. The spacing between gold particles on the filaments ranged from ~30–90 nm but was most commonly between 60–65 nm (Fig. 9 C).

Discussion

The purpose of this study was to visualize KLP61F within mitotic spindles of *Drosophila* syncytial blastoderms, in order to determine whether KLP61F acts as a MT-MT sliding motor involved in spindle pole separation or if it cross-links MTs to a spindle matrix and organizes the poles. To this end, we immunolocalized KLP61F in mitotic spindles using immunofluorescence and immunoEM and we performed a detailed structural analysis of the mitotic spindle components with which KLP61F putatively associates. The results of these analyses support the hypothesis that KLP61F participates in the formation and function of bipolar mitotic spindles by cross-linking and sliding MTs in relation to one another.

Drosophila Embryonic Spindles Contain Interpolar MT Bundles, Potentially Capable of Exerting Pushing Forces on Opposite Spindle Poles

In order for a MT-MT sliding mechanism to play a role in spindle pole positioning, the half spindles must be in contact through overlapping antiparallel MTs, most likely at the spindle midzone. Yet, tubulin immunofluorescence shows little or no staining of the spindle midzone in *Drosophila* embryos. Strikingly, however, EM reveals the presence robust interpolar MT bundles running through this region to bridge together the half spindles. Reconstruction of a representative interpolar bundle from serial cross-sections indicates that they consist of two MT arrays emanating from opposite poles that interdigitate in the midzone region. The region of antiparallel MT interdigitation extends ~1 μm into each half spindle and, thus, motor proteins that drive MT-MT sliding within these interpolar MT bundles could play a role in spindle pole positioning. For example, plus-end-directed motors could cross-link and slide apart antiparallel MTs in the region of interdigitation resulting in a repulsion of the poles (outward force), while minus-end-directed motors could pull the poles together (inward force).

The morphological characteristics of *Drosophila* embryonic spindles are consistent with the exertion of such counterbalancing forces. Since MTs will grow as straight tubes in the absence of an external force, the curvature of the interpolar MT bundles on the perimeter of the fusiform metaphase and anaphase A spindles (Fig. 1, B and C) suggests that they are being subjected to compressive forces resulting from a counterbalance of antagonistic forces pulling the poles inward and pushing them outward. An abrupt change in this counterbalance appears to coincide with the onset of anaphase B, which is characterized by straightening of interpolar MTs (Fig. 1 D). In such a scenario, a release of the inward force would relax the compressive forces acting on MTs allowing the poles to be pushed apart. A similar counterbalance of forces involving

bipolar kinesins has been proposed for *S. cerevisiae* (Saunders et al., 1997b), *S. pombe* (Pidoux et al., 1996), and *A. nidulans* (O'Connell et al., 1993).

KLP61F Is Appropriately Positioned to Slide Apart Antiparallel MTs

The hypothesis that KLP61F functions by cross-linking and sliding spindle MTs apart is supported by the observations that a severe loss-of-function mutation in the gene encoding KLP61F results in a late larval lethal phenotype, hallmarked by monoastral spindles in proliferating cells (Heck et al., 1993) and that the native KLP61F holoenzyme is a bipolar homotetramer, capable of cross-linking adjacent MTs and sliding them in relation to one another (Cole et al., 1994; Kashina et al., 1996a,b). To test this model, it is essential to determine the structural basis of the interaction between KLP61F motors and the mitotic spindle. The immunolocalization of KLP61F provides data relevant to this issue by revealing that KLP61F associates with spindle MTs in a phosphorylation dependent fashion, that it associates directly with interpolar MT bundles, and, strikingly, that bipolar KLP61F motors cross-link MTs within these bundles.

Phosphorylation of KLP61F by cdk1/CyclinB Targets KLP61F to Mitotic Spindles

Work on the bipolar Eg5 kinesin in humans and frogs has shown that the phosphorylation of bipolar Eg5 kinesin motors by cdk1/cyclinB at a specific site in the BCB targets these motors to spindles. Similarly, our results show that KLP61F associates with the spindle when phosphorylated in the BCB. This contrasts with the results from studies on the bipolar kinesins from the budding yeast *S. cerevisiae* that lack BCBs (Heck et al., 1993) and fission yeast *S. pombe* where the phosphorylation of this site does not affect the spindle association of the motor (Drummond et al., 1998). The significance of this difference is unclear but may reflect the fact that in both types of yeast, mitosis occurs completely within the confines of the nuclear envelope so that mitotic motors can interact with spindle MTs but not cytoplasmic MTs. However, in most other systems the spindle forms in the cytoplasm and precocious contact between mitotic motors and cytoplasmic MTs might perturb interphase MT arrays.

In *Drosophila* early embryos, the nuclear envelope never completely breaks down but instead fenestrates only at the points where spindle MTs enter the nuclear region. Our results showing that phospho-KLP61F associates with nuclei and spindles while nonphosphorylated KLP61F is excluded from these compartments, suggest that phosphorylation serves to sequester an active pool of the motor in a compartment where it can contact spindle MTs but not cytoplasmic MTs. How phosphorylation regulates the localization of KLP61F is unknown. It does not appear to do so by inducing the formation of bipolar tetramers, as our hydrodynamic analyses show that both phospho- and unphospho-KLP61F motors are predominantly tetrameric (Table I). It is also possible that phosphorylation increases the processivity of KLP61F motor activity that would, in turn, increase the time the motor spends associated with MTs. However, data regarding this are lacking. Clearly, the mechanism of the phospho-regulation of KLP61F localization and function requires additional investigation and will not be discussed further here.

KLP61F Is Concentrated on Interpolar MT Bundles

Our data show a clear association of KLP61F with interpolar MT bundles, visible as thin filaments of phospho-KLP61F bridging the midzone during both metaphase and anaphase by immunofluorescence (Fig. 6) that colocalize with interpolar MT bundles (Fig. 7). Interestingly, double label immunofluorescence images also show that the concentration of KLP61F is disproportionately high on MT bundles in the midzone and disproportionately low at the poles and on astral MTs when compared with tubulin staining. (Whole mount immunofluorescence provides a superior method for comparing the concentrations of motors and microtubules than does immunoEM of ultrathin sections, so the relative enrichment for KLP61F in these bundles is not apparent in Fig. 8.) This pattern shows a striking correspondence with the region of half spindle interdigitation within interpolar MT bundles suggesting that phospho-KLP6F has a particular affinity for antiparallel MTs (conversely, KLP61F could have an affinity specifically for the plus-ends of spindle MTs). However, it should be noted that other factors, such as the masking of both tubulin and phospho-KLP61F antigenic sites within the midzone might also affect the relative intensity of their fluorescence; for example, if the masking of tubulin and KLP61F antigenic sites in this region is nonequivalent, the ratio of their fluorescence intensities would not mirror their relative concentrations. We note, however, that the region of the spindle showing disproportionately high phospho-KLP61F fluorescence intensity extends ~1–2 μm into each half spindle, well beyond the zone of potential antigenic masking, indicating that the concentration of KLP61F in regions of MT interdigitation is truly disproportionately high.

KLP61F Is a Bipolar MT-MT Cross-linker

Whereas immunofluorescence reveals a general colocalization of KLP61F with interpolar MT bundles, immunoEM shows a close juxtaposition of the motor with the MTs within these bundles. At low magnification the immunolabeling pattern is obviously linear, similar to that expected from a microtubule stain. At higher magnifications, the gold particles are clearly aligned along MTs, and closely juxtaposed to the MT surfaces (Table II). Since our phospho-KLP61F antibody recognizes an epitope in the tail domain of the motor, this close juxtaposition of gold particles and MTs strongly suggests that the tail is positioned adjacent to a motor domain (see Fig. 9 A). The average distance between gold particles and the MT surface is ~10 nm, approximately the diameter of a KLP61F motor domain, supporting this suggestion. Furthermore, the analysis of the deduced sequence of KLP61F together with rotary shadowing EM analysis of the native holoenzyme, place the BCBs at the opposite end of an α-helical rod spaced ~60 nm apart, consistent with the model shown in Fig. 9 A.

Direct evidence in support of MT-MT cross-linking by bipolar KLP61F motors was obtained by visualizing gold

decorated spindles after digital enhancement of contrast. In the images shown in Fig. 9 B, for example, gold-labeled phospho-BCBs clearly associate with electron-dense crossbridges at a spacing of ~60 nm, in strong support of our previously proposed structural model for KLP61F. The average distance of 10 nm between the gold-labeled BCB and the MT surface (discussed above) summed with the ~60 nm spacing between the gold particle clusters on individual crossbridges, suggests a spacing between cross-linked MTs of ~80 nm, consistent with the relatively wide spacing between antiparallel MTs within interpolar MT bundles (Fig. 3 C). However, KLP61F is also clearly present in regions of the interpolar MT bundles that contain only parallel MTs, in which cross-links of a similar length (~60 nm) are also observed. Therefore, these data are most consistent with the idea that bipolar KLP61F motors cross-link both parallel and antiparallel MTs but other factors (MAPs or motors) must contribute to the generally closer packing of nearest neighbor MTs observed within parallel MT bundles (Fig. 3 B). Moreover, the close spacing of parallel MTs near the poles suggests that in this region of the spindle, KLP61F motors must cross-link parallel MTs that are not nearest neighbors. Further testing of this hypothesis requires a more thorough understanding of the organization of parallel vs. antiparallel MTs within interpolar MT bundles.

Model for KLP61F Function in the Spindle

Based on the localization of KLP61F shown here, its transport properties, and the phenotype of severe loss of function mutants, we propose the following expanded model for KLP61F function (shown schematically in Fig. 10). During centrosome migration, KLP61F is active and homotetrameric but sequestered away from MTs within the intact nuclear envelope. As the nuclear envelope fenestrates during prometaphase and MTs enter the nuclear region, KLP61F is free to bind and cross-link parallel and antiparallel spindle MTs, alike, riding slowly toward their plus-ends. The ability of KLP61F to cross-link MTs of both polarities assumes that theKLP61F motor domain is capable of swiveling 360° as has been shown for conventional kinesin (Hunt and Howard, 1993). Because of the plus-end–directed motility of KLP61F, a steady state is established in which KLP61F is present throughout the spindle but concentrated in the midzone, where the plus-ends of MTs from both half spindle interdigitate. The interaction of KLP61F with parallel MTs results in the formation of MT bundles capable of capturing kinetochores or interacting with MT bundles emanating from the opposite pole but, since the force vector on both MTs is the same, no net MT-MT sliding occurs. Conversely, when KLP61F interacts with antiparallel MTs, cross-linked MTs slide apart, generating an outward force on the poles. During metaphase and anaphase A, this force produces isometric tension counterbalancing an inward force to hold the poles apart. As the antagonistic inward force is released during anaphase B, the outward force serves to drive the poles apart. In other systems, where anaphase B involves strong pulling forces on the poles (Kronebusch and Borisy, 1982; Aist et al., 1993), the MT-MT interactions mediated by KLP61F might also serve as a brake, regulating the rate of spindle elongation.

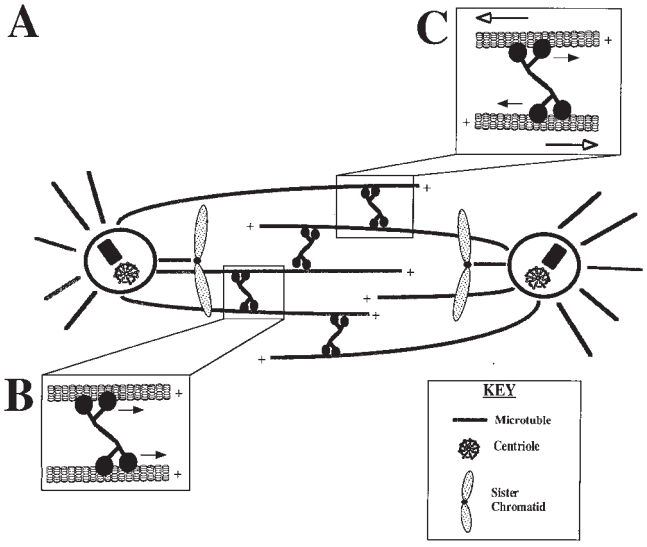

Figure 10. Model for KLP61F function. (A) As the nuclear envelope fenestrates and MTs enter the nuclear region, KLP61F cross-links spindle MTs regardless of orientation and rides toward their plus ends thereby becoming concentrated in the midzone. (B) If KLP61F cross-links parallel MTs they will be organized into bundles but no MT-MT sliding will be generated. (C) If KLP61F cross-links antiparallel MTs, the force generated by KLP61F will push the MTs apart. This results in isometric forces that hold the poles apart during metaphase and anaphase A, and isotonic forces that drive spindle elongation during anaphase B.

While our data clearly show KLP61F cross-linking interpolar MTs, it does not directly address several important issues. First, implicit in this model is that centrosome migration during prophase does not involve KLP61F, since this occurs before nuclear envelope fenestration when the motor is sequestered in the nucleus (Fig. 1 A). While we cannot exclude the possibility that the low level of KLP61F present in the cytoplasm is sufficient to drive prophase centrosome migration, it is also conceivable that spindle formation proceeds normally before nuclear envelope fenestration in the absence of KLP61F function and that the monoastral spindles seen in KLP61F mutants result from the collapse of a preformed bipolar spindle. It should be noted that such a spindle collapse has been observed in *S. cerevisiae* mutants carrying null alleles for the bipolar kinesins, cin8 and kip1 (Saunders et al., 1997). Moreover, although the monoastral spindles observed in bipolar kinesin mutants in *A. nidulans* (Enos and Morris, 1990), and *S. pombe* (Hagan and Yanagida, 1990) have been interpreted as resulting from defects in the initial separation of the spindle poles during spindle assembly, one cannot rule out the possibility that these structures result from the collapse of already assembled spindles. Direct visualization of spindle formation in KLP61F mutants should help resolve precisely when KLP61F function is needed. Second, although we have not observed KLP61F concentrated on kinetochore MT bundles or associated with a spindle matrix we cannot rule out the possibility that such interactions can occur at least in some systems.

The bipolar kinesin, KLP61F is critically important for mitosis. The data reported here, in concert with the motil-

ity properties of the motor and the phenotype of severe loss of function mutants, strongly suggest that KLP61F functions in a sliding filament mechanism to hold the spindle poles apart during metaphase and anaphase A and to drive spindle elongation during anaphase B. Given the strikingly similar molecular architecture of myosin II and KLP61F, it is appealing to speculate that the bipolar configuration of force generating enzymes involved in the sliding of cytoskeletal filaments is highly conserved and a fundamental feature of cytoskeletal activity.

The p-BCB antibody project was initiated while J.M. Scholey was on sabbatical in the Department of Biochemistry and Biophysics at UCSF and he thanks the members of the Alberts, Mitchison, Vale, and Walter labs for their hospitality. The authors gratefully acknowledge Dr. Larry Goldstein for discussions and for supplying anti-recombinant KLP61F antibody. We would also like to thank members of the Scholey lab and particularly Greg Rogers for Fig. 10 and Dana Rashid for help with photographic development. Finally, we would like to thank Rick Harris, director of the UCD Section of Molecular and Cellular Biology Microscopy Center for help in numerous areas of the project.

This work was supported by National Institutes of Health (NIH) grant number GM55507 to J.M. Scholey, and D.J. Sharp was supported by NIH postdoctoral fellowship number GM19262.

Received for publication 19 August 1998 and in revised form 30 November 1998.

References

Aist, J.R., H. Liang, and M.W. Berns. 1993. Astral and spindle forces in PtK2 cells during anaphase B: a laser microbeam study. *J. Cell Sci.* 104:1207–1216.

Ashburner, M. 1989. *Drosophila*: A Laboratory Handbook. Cold Spring Harbor Laboratory Press, Cold Spring Harbor, NY. 503–519.

Barton, N.R., A.J. Pereira, and L.S.B. Goldstein. 1995. Motor-activity and mitotic spindle localization of the *Drosophila* kinesin-like protein KLP61F. *Mol. Biol. Cell.* 6:1563–1574.

Barton, N.R, and L.S.B. Goldstein. 1996. Going mobile: microtubule motors and chromosome segregation. *Proc. Natl. Acad. Sci. USA.* 5:1735–1742.

Brinkley, B.R. 1990. Toward a structural and molecular definition of the kinetochore. *Cell Motil. Cytoskel.* 16:104–109.

Cole, D.G., W.M. Saxton, K.B. Sheehan, and J.M. Scholey. 1994. A 'slow' homotetrameric kinesin-related protein purified from *Drosophila* embryos. *J. Biol. Chem.* 269:22913–22916.

Desai, A., and T.J. Mitchison. 1995. A new role for motor proteins as couplers to depolymerizing microtubules. *J. Cell Biol.* 128:1–4.

Drummond, D.R., and I.M. Hagan. 1998. Mutations in the BCB of Cut7 indicate divergence of regulation within the bimC family of kinesin-related proteins. *J. Cell. Sci.* 111:853–865.

Enos, A.P., and N.R. Morris. 1990. Mutation of a gene that encodes a kinesin-like protein blocks nuclear division in *Aspergillus nidulans*. *Cell.* 60:1019–1027.

Euteneuer, U., W.T. Jackson, and J.R. McIntosh. 1982. Polarity of microtubules in *Haemanthus* endosperm. *J. Cell Biol.* 94:644–653.

Gelfand, V., and J.M. Scholey. 1992. Every motion has its motor. *Nature.* 359: 480–482.

Hagan, I., and M. Yanagida. 1990. Novel potential mitotic motor protein encoded by the fission yeast $Cut7^{+}$ gene. *Nature.* 347:563–566.

Hagan, I., and M. Yanagida. 1992. Kinesin-related Cut7 protein associates with mitotic and meiotic spindles in fission yeast. *Nature.* 356:74–76.

Heck, M.M., A. Pereira, P. Pesavento, Y. Yannoni, A.C. Spralding, and L.S.B. Goldstein. 1993. The kinesin-like protein KLP61F is essential for mitosis in *Drosophila*. *J. Cell Biol.* 123:665–679.

Hoyt, M.A. 1994. Cellular roles of kinesin and related proteins. *Cur. Opin. Cell Biol.* 6:63–68.

Hoyt, M.A., L. He, K.K. Loo, and W.S. Saunders. 1992. Two *Saccharomyces cerevisiae* kinesin-related gene-products required for mitotic spindle assembly. *J. Cell Biol.* 118:109–120.

Hunt, A.J., and J. Howard. 1993. Kinesin swivels for microtubule movement in any direction. *Proc. Natl. Acad. Sci. USA.* 90:11653–11657.

Kashina, A.S., R.J. Baskin, D.G. Cole, K.P. Wedaman, W.M. Saxton, and J.M. Scholey. 1996a. A bipolar kinesin. *Nature.* 379:270–272.

Kashina, A.S., J.M. Scholey, J.D. Leszyk, and W.M. Saxton. 1996b. An essential bipolar mitotic motor. *Nature.* 384:225.

Kashina, A.S., G.C. Rogers, and J.M. Scholey. 1997. The bimC family of kinesins: essential bipolar mitotic motors driving centrosome separation. *Biochim. Biophys. Acta.* 1357:257–271.

Kiss, J.Z., and L.A. Staehelin. 1995. High pressure freezing. *In* Rapid Freezing, Freeze Fracture and Deep Etching. N.J. Severs and D.M. Shotton, editors. Wiley-Liss Inc., New York. 89–104.

Kronebusch, P.J., and G.G. Borisy. 1982. Mechanics of anaphase B movement. *In* Biological Functions of Microtubules and Related Structures. H. Sakai, H. Mohri, and G.G. Borisy, editors. Academic Press, New York. pp. 233–245.

Mastronarde, D.N., K.L. McDonald, R. Ding, and J.R. McIntosh. 1993. Interpolar spindle microtubules in PTK cells. *J. Cell Biol.* 123:1475–1489.

McDonald, K.L. 1994. Electron microscopy and EM immunocytochemistry. *Methods Cell Biol.* 44:411–444.

McDonald, K.L., J.D. Pickett-Heaps, J.R. McIntosh, and D.H. Tippit. 1977. On the mechanism of anaphase spindle elongation in *Diatoma vulgare*. *J. Cell Biol.* 74:377–388.

McIntosh, J.R., P.K. Hepler, and D.G. Van Wie. 1969. Model for mitosis. *Nature.* 224:659–663.

McIntosh, J.R., and S.C. Landis. 1971. The distribution of spindle microtubules during mitosis in cultured human cells. *J. Cell Biol.* 49:468–497.

Meyer, D., D. Rines, A.S. Kashina, D.G. Cole, and J.M. Scholey. 1998. Purification of novel kinesins from embryonic systems. *Methods Enzymol.* 298:133–153.

O'Connell, M.J., P.B. Meluh, M.D. Rose, and M.R. Morris. 1993. Suppression of the bimC mitotic spindle defect by deletion of klpA, a kar3 related kinesin like protein in *Aspergillus nidulans*. *J. Cell Biol.* 120:153–162.

Oegema, K., W.G. Whitfield, and B.M. Alberts. 1995. The cell cycle-dependent localization of the CP190 centrosomal protein is determined by the coordinate action of two separable domains. *J. Cell Biol.* 131:1261–1273.

Pidoux, A.L., M. LeDizet, and W.Z. Cande. 1996. Fission yeast pkl1 is a kinesin-related protein involved in mitotic spindle function. *Mol. Biol. Cell.* 7:1639–1655.

Roof, D.M., P.B. Meluh, and M.D. Rose. 1992. Kinesin-related proteins required for assembly of the mitotic spindle. *J. Cell Biol.* 118:95–108.

Saunders, W.S., and M.A. Hoyt. 1992. Kinesin-related proteins required for structural integrity of the mitotic spindle. *Cell.* 70:451–458.

Saunders, W.S., D. Koshland, D. Eshel, I.R. Gibbons, and M.A. Hoyt. 1995. *Saccharomyces cerevisiae* kinesin- and dynein-related proteins required for anaphase chromosome segregation. *J. Cell Biol.* 128:617–624.

Saunders, W., D. Hornack, V. Lengyel, and C. Deng. 1997a. The *Saccharomyces cerevisiae* kinesin-related motor Kar3p acts at preanaphase spindle poles to limit the number and length of cytoplasmic microtubules. *J. Cell Biol.* 137: 417–431.

Saunders, W., V. Lengyel, and M.A. Hoyt. 1997b. Mitotic spindle function in *Saccharomyces cerevisiae* requires a balance between different types of kinesin-related motors. *Molecular Biol. Cell.* 8:1025–1033.

Sawin, K.E., K. Leguellec, M. Phillipe, and T.J. Mitchison. 1992. Mitotic spindle organization by a plus-end-directed microtubule motor. *Nature.* 359:540–543.

Sawin, K.E., and T.J. Mitchison. 1995. Mutations in the kinesin-like protein Eg5 disrupting localization to the mitotic spindle. *Proc. Nat. Acad. Sci. USA.* 92: 4289–4293.

Stafstrom, J.P., and L.A. Staehelin. 1984. Dynamics of the nuclear envelope and of nuclear pore complexes during mitosis in the *Drosophila* embryo. *Eur. J. Cell Biol.* 34:179–189.

Steinbrecht, R.A., and M. Muller. 1987. Freeze substitution and freeze drying. *In* Cryotechniques in Biological Electron Microscopy. R.A. Steinbrecht and K. Ziergold, editors. Springer-Verlag, Berlin. 149–172.

Stierhof, Y., H. Schwartz, M. Durrenburger, W. Villiger, and E. Kellenberger. 1991. Yield of immunolabel compared to resin sections and thawed cryosections. *Colloidal Gold: Principles, Methods, and Applications.* 3:87–115.

Straight, A.F., J.W. Sedat, and A.W. Murray. 1998. Time-lapse microscopy reveals unique roles for kinesins during anaphase in budding yeast. *J. Cell Biol.* 143:687–694.

Theurkauf, W.E. 1994. Immunofluorescence analysis of the cytoskeleton during oogenesis and early embryogenesis. *Methods Cell Biol.* 44:489–505.

Walczak, C.E., and T.J. Mitchison. 1996. Kinesin-related proteins at mitotic spindle poles-function and regulation. *Cell.* 85:943–946.

Winey, M., C.L. Mamay, E.T. O'Toole, D.N. Mastronarde, T.H. Giddings, Jr., K.L. McDonald, and J.R. McIntosh. 1995. Three-dimensional ultrastructural analysis of the *Saccharomyces cerevisiae* mitotic spindle. *J. Cell Biol.* 129: 1601–1615.

Wright, B.D., M. Terasaki, and J.M. Scholey. 1993. Roles of kinesin and kinesin-like proteins in sea urchin embryonic cell division: evaluation using antibody microinjection. *J. Cell Biol.* 123:681–689.